SYMBOL ERROR RATE OF GENERALIZED SELECTION COMBINING WITH SIGNAL SPACE DIVERSITY IN RAYLEIGH FADING CHANNELS

A. Essop* and H. Xu**

** School of Engineering, University of Kwa-Zulu Natal, King George V Avenue, Durban, South Africa. E-mail: eaadil3@yahoo.com, aadil3e@gmail.com*
*** School of Engineering, University of Kwa-Zulu Natal, King George V Avenue, Durban, South Africa. E-mail: xuh@ukzn.ac.za*

Abstract: This paper concerns M-ary quadrature amplitude modulation (M-QAM) with signal space diversity (SSD) and generalised selection combining (GSC) in independent and identically distributed (i.i.d) Rayleigh fading channels. The theoretical symbol error rate (SER) performance in i.i.d Rayleigh fading channels for M-QAM with SSD and GSC is derived. The theoretical SER performance of M-QAM with SSD and GSC reception is confirmed via simulations. Thereafter, the diversity gain of M-QAM with SSD and GSC is also analysed. Finally the signal-to-noise ratio (SNR) gap of M-QAM with SSD between selection combining (SC) and maximal ratio combining (MRC) is investigated and validated via simulations.

Keywords: Generalized Selection Combining (GSC), Signal Space Diversity (SSD), M-ary quadrature amplitude modulation (M-QAM).

1. INTRODUCTION

Over the last decade there has been a substantial increase in the number of wireless devices that utilise wireless connectivity with a large bandwidth. This drives a demand to improve wireless communications. In wireless communications, multipath fading is one of the main factors contributing to a decrease in bit error rate (BER) and/or symbol error rate (SER) performance. The application of diversity into a wireless communication system can play a role in improving BER and/or SER performance [1].

The use of rotated signal constellations results in the addition of diversity into a system. This diversity is more commonly known as signal space diversity (SSD) and by adding SSD into a wireless communication system the BER or SER performance can improve [2, 3]. SSD can be thought of as a conventional M-ary quadrature amplitude modulation (M-QAM) constellation, rotated by a certain angle. Rotating the constellation would allow any two constellation points to achieve a maximum number of distinct components (constellation coordinates) [2, 3]. With the addition of component interleaving each of the components is affected by independent fading [3, 4]. As a result, SSD offers superior immunity to noise as there is a low probability that any two points will collapse at the same time [2, 3].

Receiver diversity can also be used to improve BER or SER performance. Receive diversity effectively provides multiple signal paths. This particular diversity technique takes advantage of the low probability that deep fading is unlikely to occur simultaneously on all signal paths [1]. Maximal ratio combining (MRC) and selection combining (SC) are two commonly used techniques which take advantage of multiple paths [5]. MRC offers superior performance at the cost of high implementation complexity since the receiver needs to estimate and combine all paths. SC has a lower implementation complexity since the receiver only needs to estimate all paths and select one path, but the low complexity of SC results in poorer performance. To trade-off between performance and complexity a hybrid selection combining scheme can be used [1]. This hybrid selection combining scheme is more commonly known as generalized selection combining (GSC). In GSC, a subset of receive antennas are selected based on each receiver path's signal-to-noise ratio (SNR). This subset is then combined using MRC. GSC is typically expressed as GSC (L_C, L), where L is the total number of receive antennas and L_C is the number of receive antennas which are being combined ($L_c \leq L$). GSC will result in MRC when $L_c = L$ and similarly SC when $L_C = 1$. GSC ($L_c < L$) offers lower complexity at the cost of performance reductions when compared to MRC. It is typically applied to offer a decrease in complexity whilst still providing BER/SER performance enhancements.

Implementing SSD together with receiver diversity introduces additional diversity and improves BER or SER performance. Receiver diversity with SSD was previously considered in [6], where SSD with MRC in Rayleigh fading channels was investigated. MRC has higher resource requirements when compared to SC, such as power consumption and processing speeds. GSC allows for MRC to be used when required or a suboptimal choice between MRC and SC. This makes GSC more feasible, as it allows the user to select an option to favourably use available resources. For example in

portable applications, battery capacity can be a weak point. A system which applies variable GSC, depending on bandwidth load or signal strength can save significant battery power and other system resources.

To the authors' best knowledge M-QAM with SSD and GSC has not been discussed in literature. This motivates us to investigate the SER performance of M-QAM with SSD and GSC reception in this paper. For the purpose of this paper only square M-QAM constellations will be considered.

In a SSD system, the BER or SER depends on the rotation angle of the constellation points. This paper highlights two previously applied methods to derive an optimal rotation angle, namely the minimum product distance (MPD) and the design criterion [6-8]. In this paper the design criterion refers to the criterion of minimum Euclidean distance (MED) on the compound constellation. The main focus of this paper is to extend the approach in [6] to derive a closed form expression for the SER of M-QAM with SSD and GSC reception, which has not been presented in current literature.

A comparison between different methods can help one to decide which method best suits an application. It is vital to know the BER or SER performance difference between the two extreme cases of GSC, as this will allow one to correctly apply a blend between SC and MRC. Diversity analysis between the two extreme cases would theoretically provide insight on the performance difference. There has not been any recent work on the diversity analysis of SSD with MRC and SC. Should the diversity analysis result in no change, it then becomes important to analyse the signal-to-noise (SNR) gap between the two extreme cases.

Previous work showing the SNR gap between SC and MRC for conventional M-QAM has been presented in [9]. However, [9] did not provide any claims as to how SSD would influence this relationship. This also motivates us to present a diversity and SNR gap investigation for M-QAM with SSD and GSC.

The paper is organised as follows: a system model will be presented in section 2. The theoretical SER performance is derived in section 3. In section 4 the diversity gain and SNR gap are analysed. Simulation results and discussions are presented in section 5. Finally section 6 draws the conclusion of the paper.

2. SYSTEM MODEL

Consider a two dimensional M-QAM SSD system as shown in Fig. 1 [6]. The information bits are firstly mapped to two conventional M-QAM symbols. These two M-QAM symbols are then rotated. Finally the rotated M-QAM symbols are interleaved prior to transmission. This can be expressed mathematically as follows:

Let the original and rotated constellation set be denoted by S and X, respectively. The rotated M-QAM symbols are given by.

$$x_i = s_i R^{\theta} \ , i \in [1:2] \tag{1}$$

where $s_i \in S, s_i = \left[s_i^I \ \ s_i^Q\right]$ and $x_i \in X, x_i = \left[x_i^I \ \ x_i^Q\right]$. $(\cdot)^I$ and $(\cdot)^Q$ are the in-phase and quadrature component of a signal, respectively, and the rotating matrix R^{θ} is given by [6]:

$$R^{\theta} = \begin{bmatrix} cos\theta & sin\theta \\ -sin\theta & cos\theta \end{bmatrix} \tag{2}$$

A pair of M-QAM rotated symbols is interleaved prior to transmission. A typical pair of interleaved symbols is given by:

$$u_1 = x_1^I + jx_2^Q \tag{3.1}$$

$$u_2 = x_2^I + jx_1^Q \tag{3.2}$$

The interleaved symbols $u_i, i \in [1:2]$, are transmitted in two subsequent time slots by a single transmit antenna over L receive antennas. Each symbol is transmitted at different time slots; however a pair of symbols needs to be received prior to retrieving the sent data, due to the interleaving, as de-interleaving is required.

Let the received symbols at antenna l and at time slot i be denoted by r_{il}, where $i \in [1:2], l \in [1:L]$. r_{il} can be given by:

$$r_{il} = h_{il} u_i + n_{il} \tag{4}$$

where n_{il} is the additive white Gaussian noise (AWGN) with distribution $CN\sim(0, N_0)$. h_{il} is the fading amplitude of the channel which can be modelled according to the Rayleigh distributed random variable with distribution given by equation (5):

$$f(h_{il}) = 2h_{il} \exp(-h_{il}^2) \tag{5}$$

where $E[\, h_{il}^2] = 2\sigma^2 = 1$

Assume that full channel state information is available at the receiver. The symbols pass an in/de-interleaving process followed by GSC at the receiver. Maximum likelihood (ML) detection will be used to estimate the received symbols. A summary of the system can be viewed in Fig. 1.

of CRCCC sequences are maintained. Therefore, by assigning an extended flock of CRCCCs to a single user, it is possible to provide significant increase in rate and spectral efficiency. The grouping of sequences belonging to an extended flock is further motivated by the ability to decode groups of sequences in a single FFT operation. This is achieved by performing fast correlation according to:

$$R_{\mathbf{r},\mathbf{c}_k^0} = \sum_{m=1}^{M} \mathcal{F}^{-1}\left\{\mathcal{F}\{\mathbf{r}^{(m)}\} \cdot \left[\mathcal{F}\left\{\mathbf{c}_{m,k}^0\right\}\right]^*\right\}, \quad (4)$$

where $\mathcal{F}[.]$ and $\mathcal{F}^{-1}[.]$ represents the FFT and IFFT operations, respectively, (.)* denotes the complex conjugate and $\mathbf{r}^{(m)}$ is the mth sequence of received symbols corresponding to the mth element code. Each symbol in the resulting sequence is a sufficient statistic for the detection of the data transmitted using one of the cyclically rotated extension sequences corresponding to the decoding sequence $c_k^0 = [c_{1,k}^0\ c_{2,k}^0\ \ldots\ c_{M,k}^0]$ (i.e., the original parent code of the CRCCC extended flock). The index of the decision variable corresponds to the number of cyclic chip rotations that was performed on the parent flock.

2.2 *Space-time orthogonal frequency division multiplexing*

The CRCCCs have been shown to perform identical to BPSK in a single antenna environment [8]. This is extended to the multi-antenna environment in this paper, by employing the combination of OSTB and space-time-frequency OFDM (STF-OFDM). This approach achieves a diversity order of $N_{Tx}N_{Rx}$, i.e., the product of the number of transmit and receive antennas, as opposed to a diversity order of N_{Rx} in the case of spatial multiplexing. However, there is a compromise to be made: spatial multiplexing yields large capacity gains predicted for multiple antennas when $N_{Rx} \geq N_{Tx}$, but at the cost of an increase in non-linear detection complexity. This is normally not applicable to the forward channel where the mobile mostly uses a single antenna and also has limited computational resources. OSTBs may have reduced capacity, but it is due to this reduction that improved performance is achievable with a single receive antenna. The maximum rate achievable with OSTBCs is [9]:

$$R_{max} = \frac{m+1}{2m}, \quad (5)$$

where $N_{Tx} = 2m-1$ or $N_{Tx} = 2m$. Let $\mathbb{N}$ denote the set of all natural numbers, so that $\{m \in \mathbb{N} | m \leq 8\}$. Taking n_s blocks of data symbols and performing the modulation operations common to single antenna systems, produces a set of vectors

$$\mathbf{s}_i = \Phi \mathbf{W}^H \mathbf{C}\mathbf{d}_i \quad i = 1,2,\ \ldots\ n_s, \quad (6)$$

where $\mathbf{d}_i$ is the ith vector of digitally modulated symbols, $\mathbf{C}$ is a matrix with columns formed by the flocks of the extended CRCCC, $\mathbf{W}$ is the discrete Fourier transform matrix and Φ is a cyclic extension matrix. Taking the rows of the resulting matrix in (6) and mapping them to a sequence of matrices,

$$\{\mathbf{s}_1[n]\ \mathbf{s}_2[n]\ \ldots \mathbf{s}_{n_s}[n]\} \rightarrow \{\Phi[n]\} n = -CP, -CP+1,\ \ldots,\ N_{FFT}-1, \quad (7)$$

according to an OSTBC, the triply orthogonal modulation is completed. This mapping is mathematically equivalent to mapping the entire OFDM symbols according to the OSTBC before transmission. The index n represents the discrete time index of the MC-CDMA sequences, N_{FFT} is the FFT length (also equal to MN for the system concerned) and CP is the cyclic prefix length. The transmitter is depicted in Figure 1 and the receiver in Figure 2.

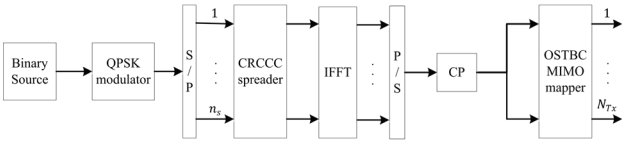

Figure 1: The modulation process performed at the transmitter

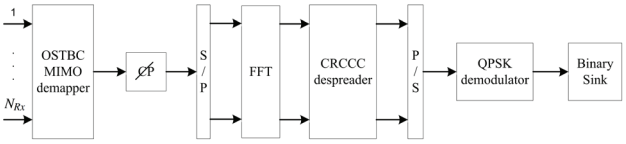

Figure 2: The demodulation process performed at the receiver

The received symbols are described by

$$\mathbf{Y}[n] = \sum_{l=0}^{L} \mathbf{H}_l \Phi[n-l] + \mathbf{N}_\sigma[n] \quad n = 0,1,\ \ldots,\ N_{FFT}-1. \quad (8)$$

The ith column of $\mathbf{Y}[n]$ corresponds to the samples received at time n during the ith OFDM symbol period (n is relative to the beginning of the symbol period), $\mathbf{H}_l$ is the lth matrix channel tap value of a length $L+1$ channel impulse response, and $\mathbf{N}_\sigma[n]$ is a matrix containing *i.i.d.* AWGN samples with zero mean and standard deviation σ_n. With this formulation of the received symbols the detection criterion for the MIMO demapping stage of the receiver is expressed as:

$$\sum_{n=0}^{N_{FFT}-1} ||\mathbf{z}[n] - \mathbf{F}[n]\hat{\mathbf{s}}[n]||^2, \quad (9)$$

where,

$$\hat{\mathbf{s}}[n] = \left[\Re\left[\hat{\mathbf{s}}^T[n]\right]\ \Im\left[\hat{\mathbf{s}}^T[n]\right]\right]^T, \quad (10)$$

$$\mathbf{z}[n] = vec\left(\mathbf{Z}[n]\right), \quad (11)$$

$$\mathbf{Z}[n] = \frac{1}{\sqrt{N_{FFT}}} \sum_{k=0}^{N_{FFT}-1} \mathbf{Y}[k] e^{-j2\pi \frac{kn}{N_{FFT}}}, \quad (12)$$

Table 1: Nearest neighbours

Points	Diagonal Neighbours	Perpendicular Neighbours
Side	2	3
Centre	4	4
Corner	1	2

Based on $P[X_A \rightarrow X_B] = P[X_A \rightarrow X_D]$ and the NN approach, the SER for rotated 16-QAM can be given as [6, 8-11] :

$$P_{SER}^{16-QAM} = 3\,P[X_A \rightarrow X_B] + 2.25\;P[X_A \rightarrow X_C] \quad (7)$$

where $P[X_A \rightarrow X_B]$ and $P[X_A \rightarrow X_C]$ are the probabilities of an error occurring due to incorrect detection of a nearby perpendicular and diagonal point, respectively.

The coordinates of X_A and X_B in Fig. 2 and Fig. 3 can be given by:

$$X_A = [3a\ 3a]\begin{bmatrix} cos\theta & sin\theta \\ -sin\theta & cos\theta \end{bmatrix} \quad (8)$$

$$X_B = [a\ 3a]\begin{bmatrix} cos\theta & sin\theta \\ -sin\theta & cos\theta \end{bmatrix} \quad (9)$$

Then the Euclidean distance between X_A and X_B, and X_A and X_C can be evaluated as follows:

$$d_{A\rightarrow B}^2 = 4a^2h_I^2\cos^2\theta + 4a^2h_Q^2\sin^2\theta \quad (10)$$

$$d_{A\rightarrow C}^2 = 4a^2h_I^2\,(1 - sin2\theta) + 4a^2h_Q^2(1 + sin2\theta) \quad (11)$$

where h_I and h_Q are the in-phase and quadrature components fading gain.

Given h_I and h_Q the conditional PEP of choosing X_B given that X_A was transmitted is given by [17]:

$$P[X_A \rightarrow X_B\,|h_I,\ h_Q] = \mathrm{Q}\left(\sqrt{\frac{d_{A\rightarrow B}^2}{2N_0}}\right) \quad (12)$$

where $Q(\cdot)$ is the Gaussian Q function.

Substituting equation (10) into (12) results in the following:

$$P[X_A \rightarrow X_B\,|\gamma_I, \gamma_Q] = Q\left(\sqrt{\frac{1}{5}\left(\gamma_I\cos^2\theta + \gamma_Q\cos^2\theta\right)}\right) \quad (13)$$

Similarly we have

$$P[X_A \rightarrow X_C\,|\gamma_I, \gamma_Q] = Q\left(\sqrt{\frac{1}{5}\left(\gamma_I\,(1 - \sin2\theta) + \gamma_Q\,(1 + \sin2\theta)\right)}\right) \quad (14)$$

where $\gamma_I = \bar{\gamma}\sum_{k=1}^{L_c}\tilde{h}_{1k}^2$ and $\gamma_Q = \bar{\gamma}\sum_{k=1}^{L_c}\tilde{h}_{2k}^2$.
$k \in [1{:}\,L_c]$. $\tilde{h}_{ik}, i \in [1{:}\,2]$, are the L_c largest channel gain of h_{il}, $l \in [1{:}\,L]$. L denotes the total number of receive antennas and $\bar{\gamma} = E[\gamma_I] = E[\gamma_Q]$ denotes the average SNR and $E[\cdot]$ denotes expectation.

The error probability $P[X_A \rightarrow X_B]$ can be obtained by averaging the conditional PEP in equation (13) over independent fading channels for GSC reception as shown in equation (15):

$$P[X_A \rightarrow X_B] = \int_0^\infty\int_0^\infty P[X_A \rightarrow X_B\,|\gamma_I, \gamma_Q]\,f_{\gamma_I}(\gamma_I)f_{\gamma_Q}(\gamma_Q)\mathrm{d}\gamma_I\mathrm{d}\gamma_Q \quad (15)$$

where f_{γ_I} and f_{γ_Q} are the PDFs for GSC in Rayleigh fading channels given by the following expression [5, Eq. 9.325].

$$f(\gamma) = \binom{L}{L_C}\left[w_1 + \frac{1}{\bar{\gamma}}w_2\,w_3\right] \quad (16)$$

where

$$w_1 = \frac{\gamma^{L_c-1}e^{-\gamma/\bar{\gamma}}}{\bar{\gamma}^{L_c}(L_c-1)!}$$

$$w_2 = \sum_{l=1}^{L-L_c}(-1)^{L_c+l-1}\binom{L-L_c}{l}\left(\frac{L_c}{l}\right)^{L_c-1}$$

and $w_3 = e^{-\frac{\gamma}{\bar{\gamma}}}\left(e^{-\frac{l\gamma}{L_c\bar{\gamma}}} - \sum_{m=0}^{L_c-2}\frac{1}{m!}\left(-\frac{l\gamma}{L_c\,\bar{\gamma}}\right)^m\right)$.

The PDF of GSC can be used to generate the PDF of SC, GSC $(1, L)$ and MRC, GSC (L, L) which are given by [5] respectively as:

$$f_{SC}(\gamma) = \frac{L}{\bar{\gamma}}\sum_{l=0}^{L-1}(-1)^l\begin{bmatrix} L-1 \\ l \end{bmatrix}e^{-\gamma\frac{1+l}{\bar{\gamma}}} \quad (17.1)$$

$$f_{MRC}(\gamma) = \frac{\gamma^{L-1}\,e^{-\frac{\gamma}{\bar{\gamma}}}}{\bar{\gamma}^L\,(L-1)!} \quad (17.2)$$

In order to evaluate and simplify the expression in equation (15), the Q function in equation (12), needs to be simplified. This is accomplished with the trapezoidal approximation of the Q function presented in [11]. The trapezoidal approximation of the Q function is given as follows [11]:

$$Q(x) = \frac{1}{2n}\left(\frac{1}{2}e^{-\frac{x^2}{2}} + \sum_{k=1}^{n-1}e^{-\frac{x^2}{2\sin^2\theta_k}}\right) \quad (18)$$

where $\theta_k = \frac{k\pi}{2n}$, n is the upper limit for the summation.

To simplify the integral found in equation (15), a moment generating function (MGF) will be used. The MGF of the output SNR is given by [5]:

$$M_y(s) = \int_0^\infty f_\gamma(\gamma)\ e^{s\gamma}\,\mathrm{d}\gamma \qquad (19)$$

The MGF for GSC can be derived using equation (18) and (19). For Rayleigh channels this is evaluated as [18, 5- Page 383 Eq. 9.321]:

$$M_{\gamma GSC}(s) = (1-s\bar{\gamma})^{-L_C+1}\prod_{l=Lc}^{L}\left(1-\frac{s\bar{\gamma}L_C}{l}\right)^{-1} \qquad (20)$$

Using equation (13) and simplifying (15) with the Q approximation - equation (18), results in the following:

$$P[X_A \rightarrow X_B] = \int_0^\infty\int_0^\infty\{\Delta_1+\Delta_2\}f_{\gamma_I}(\gamma_I)f_{\gamma_Q}(\gamma_Q)\mathrm{d}\gamma_I\mathrm{d}\gamma_Q \qquad (21)$$

where $\Delta_1 = \frac{1}{2n}\left(0.5\,e^{-\frac{0.2\left(\gamma_I\cos^2\theta+\gamma_Q\sin^2\theta\right)}{2}}\right)$,

and $\Delta_2 = \frac{1}{2n}\sum_{k=1}^{n-1}e^{-\frac{0.2\left(\gamma_I\cos^2\theta+\gamma_Q\sin^2\theta\right)}{2\sin^2\theta_k}}$.

From equation (20), the error probability equation (21), $P[X_A \rightarrow X_B]$ can be further simplified as:

$$P[X_A \rightarrow X_B] = \frac{1}{4n}M_{\gamma GSC}\left(-\frac{\cos^2(\theta)}{\varepsilon_m}\right)M_{\gamma GSC}\left(-\frac{\sin^2(\theta)}{\varepsilon_m}\right) + \frac{1}{2n}\sum_{k=1}^{n-1}M_{\gamma GSC}\left(-\frac{\cos^2(\theta)}{\varepsilon_m\sin^2(\theta_k)}\right)M_{\gamma GSC}\left(-\frac{\sin^2(\theta)}{\varepsilon_m\sin^2(\theta_k)}\right) \qquad (22)$$

where $\varepsilon_m = 10$ and ε_m is the average expected energy per symbol and this is calculated based on the M-QAM constellation size.

Similarly, $P[X_A \rightarrow X_c]$ is derived as:

$$P[X_A \rightarrow X_c] = \frac{1}{4n}M_{\gamma GSC}\left(-\frac{1+sin2\theta}{\varepsilon_m}\right)M_{\gamma GSC}\left(-\frac{1-sin2\theta}{\varepsilon_m}\right) + \frac{1}{2n}\sum_{k=1}^{n-1}M_{\gamma GSC}\left(-\frac{1+sin2\theta}{\varepsilon_m sin^2(\theta_k)}\right)M_{\gamma GSC}\left(-\frac{1-sin2\theta}{\varepsilon_m\,sin^2(\theta_k)}\right) \qquad (23)$$

Substituting equation (22) and (23) directly into equation (7) results in the SER for 16-QAM with SSD and GSC. A similar approach is used to evaluate the SER for other M-QAM constellation sizes. The perpendicular and diagonal neighbours for each constellation size are used to evaluate the coefficients of $P[X_A \rightarrow X_B]$ and $P[X_A \rightarrow X_c]$ which are denoted by A_M and B_M respectively and can be found in Table 2.

Table 2: Values for A_M, B_M and ε_m

Constellations	A_M	B_M	ε_m
4 - QAM	2	1	2
16 - QAM	3	2.25	10
64 - QAM	3.5	3.0625	42
256 - QAM	3.75	3.5156	170

The values for A_M and B_M in Table 2 are verified using the expression found in [16, Table 2] for squared M-QAM constellations.

A more general expression for GSC M-QAM SSD can be written as

$$P_{SER}^{M-QAM} = A_M P[X_A \rightarrow X_B] + B_M P[X_A \rightarrow X_c] \qquad (24)$$

where A_M, B_M and ε_m vary with each M-QAM constellation and are tabulated in Table 2.

4. DIVERSITY ORDER AND SNR GAP

Diversity analysis gives an indication of the diversity of a system. The amount of diversity effects the overall SER/BER performance of a communication system. The diversity order has not been analysed for M-QAM with SSD in current literature. This section will investigate the analysis of diversity and SNR gap between the extreme cases of GSC which are SC and MRC.

This paper will show that GSC *($L_c \neq L$)* achieves the same diversity order as MRC for conventional M-QAM due to the total available receive antennas remaining constant. However, the SER performance of GSC is worse than MRC [9]. There is in fact an SNR gap between GSC and MRC even in conventional M-QAM. The SNR gap between SC and MRC in Nakagami-m fading channels has been investigated in [9]. However, it has not commented on the SNR gap between SC and MRC for M-QAM with SSD. In this section the same approach proposed in [9] will be used to investigate the SNR gap for M-QAM with SSD.

4.1 Diversity order

Consider that the fading is independently and identically distributed with the same fading parameters and the same average SNR, $\bar{\gamma}$ for all L_c channels. For the purpose of this paper the diversity gain for the extreme cases will be derived. The extreme cases are $L_c = 1$ and $L_c = L$, which are the SC and MRC cases, respectively.

The diversity order denoted by G, of a communication system can be defined as the slope of its error probability $P_e(SNR)$ in log-scale, at values where the SNR tends to infinity [19]. This can be evaluated as follows [19]:

$$G = \lim_{\bar{\gamma}\rightarrow\infty}\frac{log[P_e(\bar{\gamma})]}{log(\bar{\gamma})} \qquad (25)$$

An approximation will be used to simplify the expression for diversity order for both MRC and SC whilst maintaining a high level of accuracy. The SER is largely dependent on the MED. At high SNR values the perpendicular closest neighbours have a greater influence on the overall SER performance when compared to diagonal neighbours. The SER derived in section 3, equation (24) can be approximated to:

$$P_{SER}^{M-QAM} \cong A_M P[X_A \rightarrow X_B] \qquad (26)$$

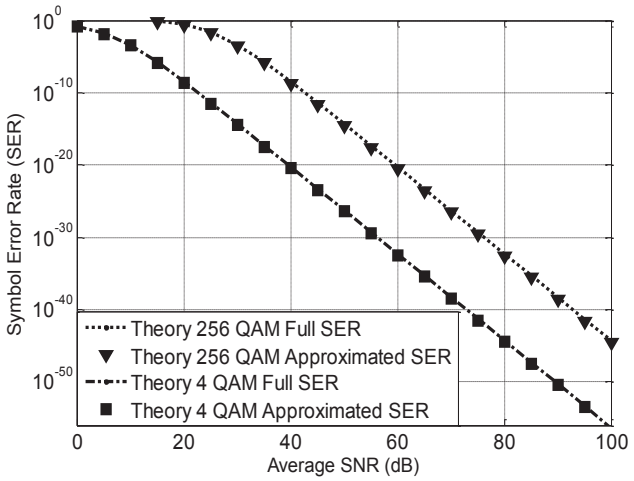

Fig. 4: SNR difference between using full SER expression and $P[X_A \rightarrow X_B]$ only for 4 and 256-QAM

The accuracy of equation (26) is questionable at first glance therefore warranting the validation of its accuracy. As per the definition of diversity order, it is evaluated as the SNR approaches infinity and it is for that reason that the above approximation maintains a high level of accuracy when calculating the diversity order. In order to quantify the error introduced using the approximation, the accuracy of equation (26) is validated by comparing it directly with its accurate counterpart, equation (24). Fig. 4 shows a direct comparison of the theoretical results between equation (24) and (26) for 4-QAM and 256-QAM SSD with GSC(3,3).

Fig. 4 illustrates that the SER approximation is constellation size independent at high SNR. Both 4-QAM and 256-QAM exhibit a similar SNR gap between equation (24) and (26), at the same respective SER. Due to the approximation being constellation size independent the accuracy errors can be evaluated for 4-QAM and hence all values of M-QAM. More details are illustrated in Fig 5.1 and Fig. 5.2, which show the performance differences for 4-QAM at low and high SNR values, respectively. The difference in SNR between equation (24) and (26) change very little across SNR values, but the percentage error would increase as the SNR values tend to zero and decrease rapidly as the SNR values tend to infinity. Fig. 5.1 and Fig. 5.2 reveal an error of 0.3 dB and 0.4 dB when operating at 18 dB and 98 dB respectively.

$$\frac{0.3\ dB}{18dB} = 1.67\ \% \qquad (27.1)$$

$$\frac{0.4\ dB}{98\ dB} = 0.48\ \% \qquad (27.2)$$

Equation (27.1) – (27.2) prove that the approximation, equation (26) is valid and holds a high level of accuracy as depicted by the miniscule error at low SNR values and even smaller error at higher SNR values. Therefore for diversity order calculations the effects of $P[X_A \rightarrow X_C]$ can be neglected.

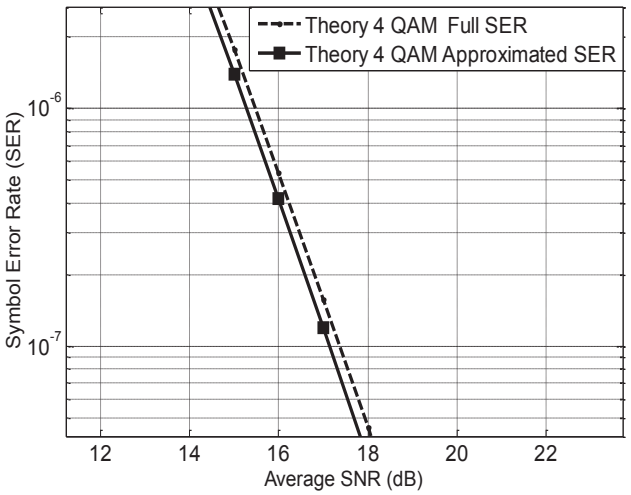

Fig. 5.1: SNR difference between using full SER expression and $P[X_A \rightarrow X_B]$ for 4-QAM at low SNR values

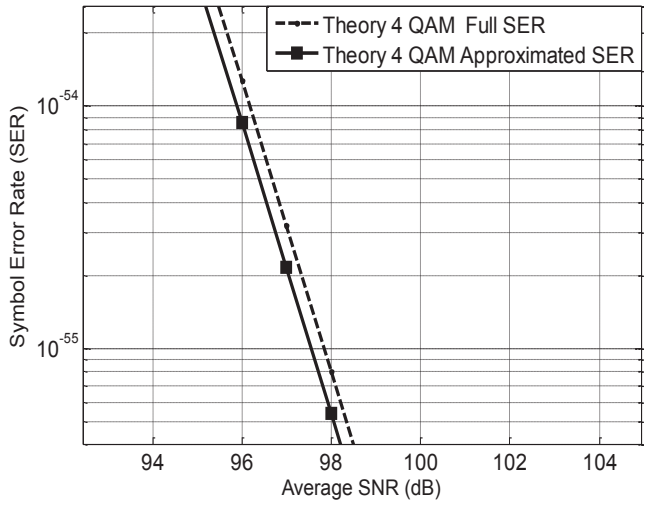

Fig. 5.2: SNR difference between using full SER expression and $P[X_A \rightarrow X_B]$ only for 4-QAM at high SNR values.

Using the approximation presented in equation (26) the diversity order for GSC $(1, L)$ and GSC (L, L) will be evaluated for L receive antennas.
The Q function in equation (15) will be simplified using the Chernoff bound found in [20] in order to simplify the diversity order calculations:

$$Q(x) \leq e^{-\frac{x^2}{2}} \qquad (28)$$

Equation (15) can be approximated using this upper bound as:

$$P[X_A \rightarrow X_B] \leq \frac{1}{2}\int_0^\infty \int_0^\infty e^{-\frac{\frac{1}{5}\left(\gamma_I \cos^2\theta + \gamma_Q \sin^2\theta\right)}{2}} f_{\gamma_I}(\gamma_I) f_{\gamma_Q}(\gamma_Q) \mathrm{d}\gamma_I \mathrm{d}\gamma_Q \qquad (29)$$

The effect introduced by the Chernoff upper bound approximation becomes negligible as the SNR approaches infinity when evaluating the diversity order.

Substituting the PDF for SC, equation (17.1) into equation (29) results in the following:

$$P[X_A \rightarrow X_B] \leq \frac{1}{2}\int_0^{\infty} e^{-\frac{1}{5}\gamma_I \cos^2\theta} \times \frac{L}{\bar{\gamma}}\sum_{l=0}^{L-1}(-1)^l \begin{bmatrix} L-1 \\ l \end{bmatrix} e^{-\gamma_I \frac{1+l}{\bar{\gamma}}} \mathrm{d}\gamma_I \times \int_0^{\infty} e^{-\frac{1}{5}\gamma_Q \sin^2\theta} \times \frac{L}{\bar{\gamma}}\sum_{l=0}^{L-1}(-1)^l \begin{bmatrix} L-1 \\ l \end{bmatrix} e^{-\gamma_Q \frac{1+l}{\bar{\gamma}}} \mathrm{d}\gamma_Q \quad (30)$$

This can be simplified as follows:

$$P[X_A \rightarrow X_B] \leq \frac{L!}{2}\left(\frac{1}{\prod_{l=1}^{L}\left(l+\frac{\bar{\gamma}}{5}\cos^2\theta\right)}\right) \times \left(\frac{L!}{\prod_{l=1}^{L}\left(l+\frac{\bar{\gamma}}{5}sin^2\theta\right)}\right) \quad (31)$$

Using the SER approximation, equation (26) and simplifying the expression above using the upper bound of $P[X_A \rightarrow X_B]$ found in equation (30) results in equation (32):

$$P_{SER} \approx A_M\, P[X_A \rightarrow X_B] = 0.5A_M(L!)^2\left(\frac{1}{\prod_{l=1}^{L}\left(l+\frac{\bar{\gamma}}{5}\cos^2\theta\right)}\right) \times \left(\frac{1}{\prod_{l=1}^{L}\left(l+\frac{\bar{\gamma}}{5}sin^2\theta\right)}\right) \quad (32)$$

Based on the definition of diversity order given in equation (25) and using equation (32) to evaluate the diversity order for GSC $(1, L)$ results in:

$$G_{SC} = \lim_{\bar{\gamma}\to\infty} \frac{log\left[A_M\, P(X_A \rightarrow X_B)^{M-QAM}\right]}{log(\bar{\gamma})} = -2L \quad (33)$$

Similar to the diversity order derivation of GSC $(1, L)$ we find the diversity order of GSC (L, L) to be:

$$G_{MRC} = \lim_{\bar{\gamma}\to\infty} \frac{log\left[A_M\, P(X_A \rightarrow X_B)^{M-QAM}\right]}{log(\bar{\gamma})} = -2L \quad (34)$$

The diversity analysis for both extreme cases of GSC results in the same diversity order. This is due to the SER difference becoming negligible as the SNR approaches infinity. This means that the diversity which is gained from all GSC cases will always be the same, as proved by the extreme cases of SC and MRC.

It becomes important to perform a SNR gap analysis between the two extreme cases of SC and MRC to provide insight on the performance differences between SC and MRC and hence GSC. The extreme cases results in a diversity order of $-2L$ each. In the next subsection the SNR gap between SC and MRC will be derived.

4.2 SNR gap

An SNR gap is defined in [9] as the difference in SNR or power that is required for that of SC and GSC to achieve the same SER when the diversity order is the same. At high SNR this gap will be constant since the slope of the SER for both SC and MRC/GSC is invariant. This paper will derive and discuss the SNR gap for SC and MRC. Adopting the approach proposed in [21], the SNR gap can be determined by the following expressions:

$$SER^{MRC}(\bar{\gamma}) = SER^{SC}(\bar{\gamma}\, G_m) \quad (35)$$

where G_m is the SNR gain. The SNR gap in dB can be evaluated as follows:

$$SNR\ gap\ (dB) = 10\log G_m \ \ dB \quad (36)$$

The exact SER equation presented in this paper is of high complexity and hence a closed form approximation is used to solve for the SNR gap. An accurate approximation of the Q function shown in equation (37) [22], will be used to derive the SER of GSC $(1, L)$ and $GSC\ (L, L)$.

$$Q(x) = \frac{1}{12}exp\left(-\frac{x^2}{2}\right) + \frac{1}{4}exp\left(-\frac{2x^2}{3}\right) \quad (37)$$

Furthermore the approximation presented in equation (26) will also be used to simply the SER expressions when evaluating the SNR gap. The accuracy of the SER expressions will not influence the SNR gain - G_m as both the SER of SC and MRC will be evaluated using the same approximations hence having its overall effect on the SNR gain and hence SNR gap nullified.

Using the PDF of SC equation (17.1) and the Q approximation, equation (37) to simplify equation (15) results in the following:

$$P[X_A \rightarrow X_B] = \left(\int_0^{\infty}\left(\frac{1}{12}e^{-\frac{A}{2}} + \frac{1}{4}e^{-\frac{2A}{3}}\right)\frac{L}{\bar{\gamma}}\sum_{l=0}^{L-1}(-1)^l \begin{bmatrix} L-1 \\ l \end{bmatrix} e^{-\gamma_I \frac{1+l}{\bar{\gamma}}} \mathrm{d}\gamma_I\right) \times \left(\int_0^{\infty}\left(\frac{1}{12}e^{-\frac{B}{2}} + \frac{1}{4}e^{-\frac{2B}{3}}\right)\frac{L}{\bar{\gamma}}\sum_{l=0}^{L-1}(-1)^l \begin{bmatrix} L-1 \\ l \end{bmatrix} e^{-\gamma_I \frac{1+l}{\bar{\gamma}}} \mathrm{d}\gamma_I\right) \quad (38)$$

where $A = \frac{2}{\varepsilon_m}\cos^2\theta$ and $B = \frac{2}{\varepsilon_m}\sin^2\theta$

Using the approximation of the SER, equation (26), which neglects the effects of the diagonal points and evaluating the integral in equation (38), gives:

$$SER^{SC} = A_m \cdot P_{SC}^1 \cdot P_{SC}^2 \quad (39)$$

where

$$P_{SC}^1 = \frac{A_m}{12}\left(\frac{L}{\bar{\gamma}}\sum_{l=0}^{L-1}(-1)^l \begin{bmatrix} L-1 \\ l \end{bmatrix}\frac{\bar{\gamma}}{\left(1+l+\frac{A\bar{\gamma}}{2}\right)}\right) + \frac{1}{4}\left(\frac{L}{\bar{\gamma}}\sum_{l=0}^{L-1}(-1)^l \begin{bmatrix} L-1 \\ l \end{bmatrix}\frac{\bar{\gamma}}{\left(1+l+\frac{2A\bar{\gamma}}{3}\right)}\right) \quad \text{and}$$

$$P_{SC}^{2} = \frac{A_m}{12}\left(\frac{L}{\bar{\gamma}}\sum_{l=0}^{L-1}(-1)^{l}\begin{bmatrix} L-1 \\ l \end{bmatrix}\frac{\bar{\gamma}}{\left(1+l+\frac{B\bar{\gamma}}{2}\right)}\right) + \frac{1}{4}\left(\frac{L}{\bar{\gamma}}\sum_{l=0}^{L-1}(-1)^{l}\begin{bmatrix} L-1 \\ l \end{bmatrix}\frac{\bar{\gamma}}{\left(1+l+\frac{2B\bar{\gamma}}{3}\right)}\right).$$

Similarly we have

$$SER^{MRC} = A_m \cdot P_{MRC}^{1} \cdot P_{MRC}^{2} \tag{40}$$

where

$$P_{MRC}^{1} = \frac{A_m}{12}\left(\left(\frac{1}{\bar{\gamma}A*\frac{1}{2}+1}\right)^{L} + \frac{1}{4}\left(\frac{1}{\bar{\gamma}A*\frac{2}{3}+1}\right)^{L}\right) \text{ and}$$

$$P_{MRC}^{2} = \frac{A_m}{12}\left(\left(\frac{1}{\bar{\gamma}B*\frac{1}{2}+1}\right)^{L} + \frac{1}{4}\left(\frac{1}{\bar{\gamma}B*\frac{2}{3}+1}\right)^{L}\right).$$

By comparing the terms found in equation (39) and equation (40) a simplification can be made. P_{MRC}^{1} can be compared directly to P_{SC}^{1} and the same applies to P_{MRC}^{2} with P_{SC}^{2}. This simplification can be used to evaluate equation (35) which results in the following

$$\left(\frac{1}{\frac{1}{2}\bar{\gamma}B+1}\right)^{L} = \left(\frac{L}{\bar{\gamma}}\sum_{l=0}^{L-1}(-1)^{l}\begin{bmatrix} L-1 \\ l \end{bmatrix}\frac{\bar{\gamma}}{\left(1+l+\frac{BG_m\bar{\gamma}}{2}\right)}\right) \tag{41}$$

Using basic mathematics, from equation (41) the value of G_m can be determined as:

$$G_m = (L!)^{\frac{1}{L}} \tag{42}$$

$$SNR\ gap_{SC-MRC} = \frac{10}{L}\log(L!)\ \ dB \tag{43}$$

The same result was obtained in [21]. This proves that the SNR gap is not related to the rotation angle or constellation size. Thus the SNR gap between a rotated and non-rotated constellation will be equal. Since the SC–MRC SNR gap is angle independent, the SNR gap for other cases of SC–GSC SNR gap is also angle independent. Hence a more general expression for the SNR gap between SC and GSC can be simplified for Rayleigh fading channel directly from [21]:

$$SNR\ gap_{SC-GSC} = \frac{10}{L}\log(L_c!\ \ (L_c)^{L-L_c})\ \ dB \tag{44}$$

where $L_c \leq L$.

The above expression provides the SNR gap for SC to any GSC system for different values of L_c. In [21], the result was derived for non-rotated constellations. Equation (43), the MRC case proved the derivation to be angle independent, therefore equation (44) can be used directly for other GSC values for rotated constellations. Furthermore equation (44) does not contain any angle or constellation size dependent variables; this concisely proves the above statement.

Equation (43) is verified by comparing simulation results with the expressions evaluation. Similarly equation (44) is also verified by simulation results. Both figures can be viewed in the results section.

5. RESULTS

The aim of this section is to validate the theoretical derivations produced in this paper through simulations. The SER performance for rotated constellations of 4, 16, 64 and 256-QAM, at the optimal angle of 31.7°, for $L_c = 1,\ 2\ ,3$ and $L = 3$ is presented. Please note the extreme cases of MRC and SC at the extreme ends of GSC is also presented in the results, i.e. $L_c = 1$ and $L_c = 3$.

The full SER expression given by (24) is graphed for each case above and compared to simulation results. This will be a means to verify the mathematical expressions as well as compare the simulated system performance with theoretical performance.

The simulated SNR gap of SC and MRC is presented to verify (43). The SNR gap between SC and MRC for $L = 1{:}5$ is verified in the results section via simulations. Thereafter the SNR gap for SC and GSC ($L_c = 1{:}L$) will be graphed for values of $L = 3{,}5$ to verify (44). The SNR gap provides more insight as to the performance compromise when switching from MRC to a specific GSC case. It would allow one to visualise the gain/loss in performance as the L_c value is increased or decreased.

The SER simulations were performed over independent and identically distributed (i.i.d) Rayleigh flat fading channels with AWGN and perfect channel estimation at the receiver.

Fig. 6-9 shows the simulated and theoretical SER performance of SSD systems with $L = 3$ and different L_c values for 4, 16, 64, and 256-QAM, respectively. All exhibit a small difference in performance between the simulation results of the SER and the theoretical SER at low SNR values (SNR < 17dB). If more than a single bit error occurred this will still count as a single SER and hence a slight difference in the theory vs. simulations at low SNR values.

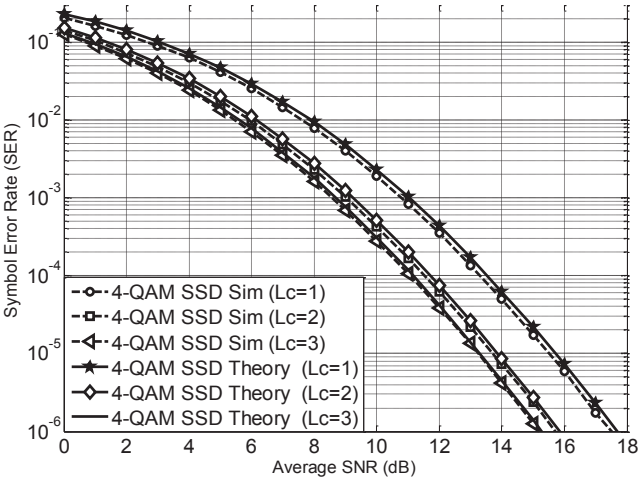

Fig. 6: SER - 4-QAM SSD with GSC in Rayleigh fading channel

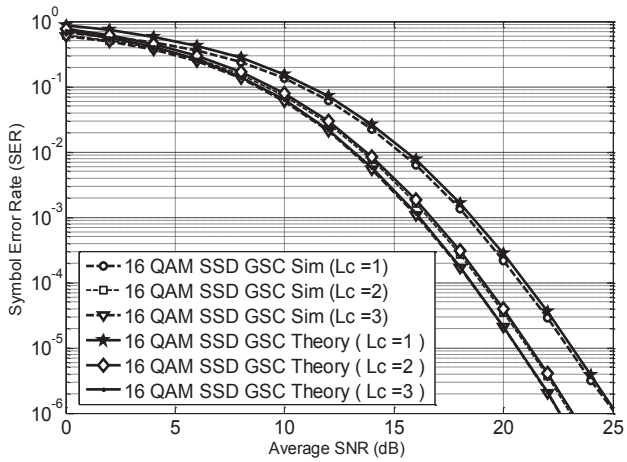

Fig. 7: SER - 16-QAM SSD with GSC in Rayleigh fading channel

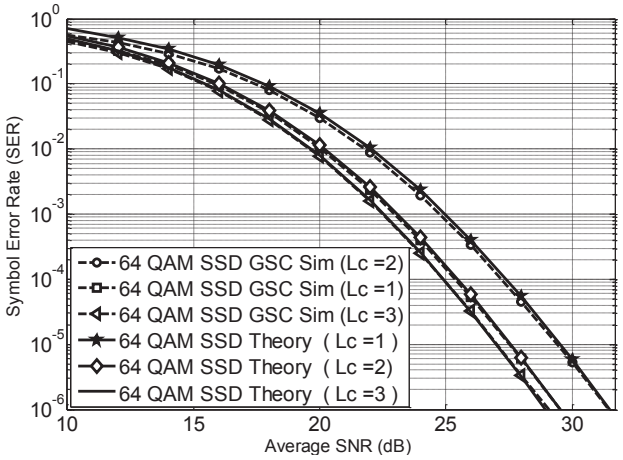

Fig. 8: SER - 64-QAM SSD with GSC in Rayleigh fading channel

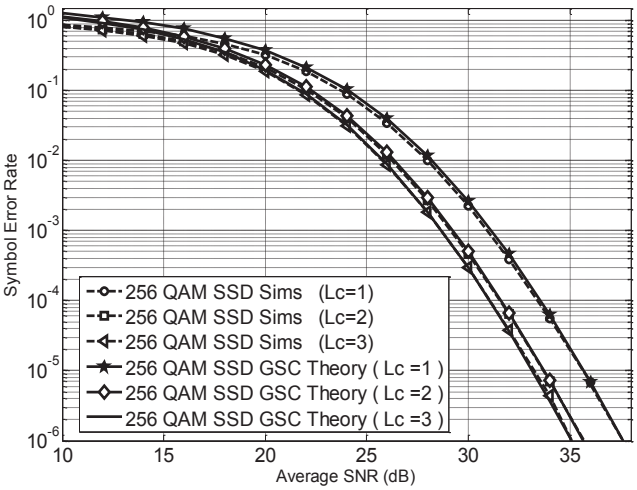

Fig. 9: SER - 254-QAM SSD with GSC in Rayleigh fading channel

At medium to high SNR the theoretical SER and simulation SER, for M-QAM in all GSC cases, closely overlap each other. This difference becomes more prominent as the constellation size increases because higher order constellations produce a greater number of errors at low SNR values and hence in practical applications the lower SNR values are seldom used, making the difference at lower SNR values unimportant.

A performance improvement as the L_c value increases from SC to MRC is also observed. By utilising a GSC scheme a designer can use this information to decide on a suitable L_c value for a device.

5.1 SNR gap relationship

The theoretical SNR gap using equation (43) and (44) are compared to actual simulation results. Due to the fact that the SNR gap is constellation size independent, the simulation results are only analysed for a 16-QAM constellation size at the optimal angle of 31.7 degrees.

Fig. 10 shows the results for the SNR gap which were derived in section 4.2. From Fig. 10 one can observe that the simulation results closely overlap the theoretical results, confirming that the relationship is true. As the number of receive antennas is increased the SNR gap between SC and MRC will increase at the same rate for M-QAM with and without SSD.

The simulations were performed at a constant SER of 10^{-7} for that of SC and MRC and the dB difference is calculated and graphed for a different number of receive antennas. At high SNR values the SER will be very small, thus making it hard to simulate. The relationship which was derived in section 4.2 holds when the SNR is substantially large (SER is low at high SNR). It is then that the SER of SC and MRC will be parallel to each other and hence a constant SNR gap between them. Due

to computational requirements and accuracy when simulating at low SER, the SNR gap has been presented for up to five receive antennas.

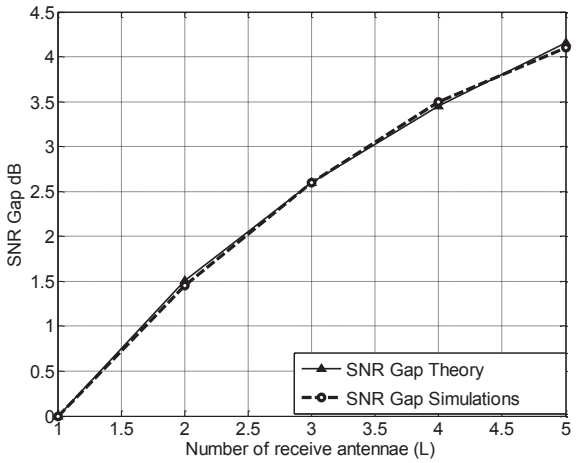

Fig. 10: SNR gap for different L values (MRC- GSC)

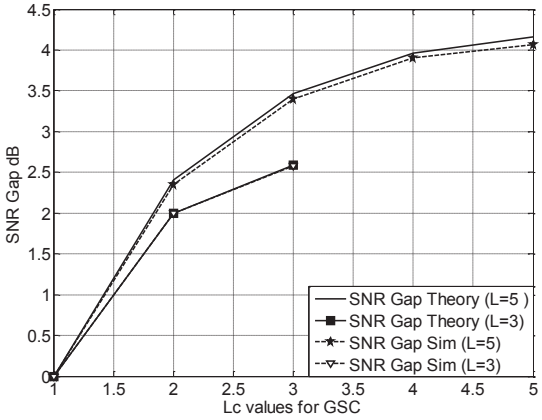

Fig. 11: SNR gap for different L_c values at $L = 3,5$

A non-linear curve representing the SNR gap between SC and MRC can be observed in Fig. 10. From the graph one can observe that when L =2 the SNR gap is 1.5 dB but when L =5 the difference is 4.1 dB.

Fig. 11 illustrates the SNR gap for different L_c values when L=5 and L=3. This is to verify equation (44) from [21] is correct. As can be seen that the SNR gap increases as L_c increases. The graph gives a visual representation of the SNR gap which is gained when switching from SC to GSC and then to MRC. As can be realized the relationship is a curve which has the least SNR gap gains when L_c approaches L. For example with L =5 and $L_c = 2$ there is an increase in the SNR gap of 2.4 dB from that of $L_c = 1$ (SC). But when $L_c = 5$ there is an increase of 0.2 dB from that of $L_c = 4$. This is useful information as one is able to realize that even though MRC is the best performing, it might not be worth the extra complexity.

6. CONCLUSION

The use of GSC on a SSD system is presented in this paper as a possible method to improve wireless communication SER performance. The SER performance of SSD using GSC with L receive antennas is derived in Rayleigh fading based on the nearest neighbour approach. A closed form solution based on the MGF function was presented in this paper.

The relationship between applying GSC ($L_c = 1$) - SC or GSC ($L_c = L$) - MRC is derived and proved to be positively related to the number of receive antennas. Similarly the power gain between SC and MRC and hence SC and GSC are presented in this paper and proved to be positively related to the number of receive antennas.

GSC proved useful as illustrated by the SNR gap curve and the small increase in performance as L_c approaches L. This was demonstrated by the small increase in the SNR gap as L_c approaches L.

The scheme presented in the paper proved to be successful as it demonstrated that the theoretical performance closely matches simulated performance and the use of GSC with SSD on an M-QAM constellation will increase SER performance.

REFERENCES

[1] H. Xu, "Symbol Error Probability for Generalized Selection Combining," *SAIEE Research Journal*, vol. 100, no. 3, pp. 68-71, Sept 2009.

[2] J. Boutros and E. Vitebro, "Signal Space Diversity: A Power-and Bandwidth- Efficient Diversity Technique," *IEEE Trans. on Info. Theory*, vol. 44, no. 4, pp. 1453 - 1467, July 1998.

[3] J. Kim and I. Lee, "Analysis of Symbol Error Rates for Signal Space Diversity in Rayleigh Fading Channels," in *IEEE International Conf. on Commun.*, Beijing, 2008, pp. 4621 - 4625.

[4] A. Chindapol, "Bit-interleaved coded modulation with signal space diversity in Rayleigh fading," in *Signals, Systems and Computers Conf.* , Pacific Grove, CA, 1999, pp. 1003-1007.

[5] M. S Alouini and M. K. Simon, *Digital Communications over Fading Channels: A Unified Approach to Performance Analysis*.: A Wiley-Interscience Publication, 2000.

[6] Z. Paruk and H. Xu, "Performance Analysis and Simplified Detection for Two - Dimensional Signal Space Diversity," *SAIEE Africa Research Journal*, vol. 104, no. 3, pp. 97-106, September 2013.

[7] S. A. Ahmadzadeh, "Signal space cooperative communication," *IEEE Trans. on wirless Commun.*, vol. 6, no. 4, pp. 1266-1271, April 2010.

[8] S. Jeon, I. Kyung, and M. K. Kim, "Component-Interleaved receive MRC with Rotated Constellation for Signal Space Diversity.," in *IEEE Conf. Veh. Technol.*, Alaska, 2009, pp. 1-6.

[9] N. Kong and L. B. Milstein, "Simple Closed Form Aymtotic Symbol Error Rate of Selection Combining and its Power Loss Compared to the Maximal Ratio Combining over Nakagami M Fading Channels," *IEEE Trans. on Commun.*, vol. 58, no. 4, pp. 1142-1150, April 2010.

[10] S. A. Ahmadzadeh, A. K. Khandani, and S.A. Motahari, "Signal Space Cooperative Communication for Single Relay Model," University of Waterloo, Ontario, Canada., Technical Report 2009.

[11] A. Saeed, T. Quazi, and H. Xu, "Hierarchical modulated quadrature amplitude modulation with signal space diversity and maximal ratio combining reception in Nakagami-m fading channels," *IET Commun.,* vol. 7, no. 12, pp. 1296-1303, Aug 2013

[12] G. Taricco and E. Viterbo, "Performance of component interleaved signal sets for fading channels," *Electronic letters*, vol. 32, no. 13, pp. 1170-1172, April 1996.

[13] I. Guillen, A. Fabregas, and E. Viterbo, "Sphere Lower Bound for Rotated Lattice Constellations in Fading Channels," *IEEE Wireless Commun.*, vol. 32, no. 13, pp. 1170-1172, April 1996.

[14] K. N. Pappi, N. D. Chatzidiamantis, and G. K. Karagiannidis, "Error Performance of Multidimensional Lattice Constellations—Part I: A Parallelotope Geometry Based Approach for the AWGN Channel," *IEEE Trans. on Commun.*, vol. 61, no. 3, pp. 1088-1098, April 2013.

[15] K. N. Pappi, "Error Performance of Multidimensional Lattice Constellations—Part II: Evaluation over Fading Channels," *IEEE Trans. on Commun.*, vol. 61, no. 3, pp. 1099-1110, April 2013.

[16] E. Salahat and I. Abualhaol "Generalized average BER expression for SC and MRC reciever over Nakagami-m fading channels," in *Personal Indoor and Mobile Radio Communications (PIMRC) 24th Int Symposium Conf.* , London, UK , 2013, pp. 3360 - 3365.

[17] M. Salehi and J. G. Proakis, *Digital Communications*, 5th ed. San Diago, USA: McGraw - Hill Higher Education, 2007.

[18] M. S. Alouini and M .K. Simon, "An MGF -Based Performance Analysis of Generalized Selection Combining over Rayleigh Fading Channels," *IEEE Trans. on Commun.*, vol. 48, no. 3, pp. 401-415, March 2000.

[19] H. Dai, H. Zhang, Q. Zhou, and B. L. Hughes, "On the Diversity Order of Transmit Antenna Selection for Spatial for Spatial Multiplexing Systems ," in *Global Telecommunications Conf.* , St. Louis, Missouri , 2005, pp. 1451-1455.

[20] U. Madhow, *Fundamentals of Digital Communication*. United Kingdom : University Press , 2008.

[21] N. Kong, S. Diego, J. C. Corp, and C. Wang, "Simple BER Approximations for Generalized Selection Combining (GSC) over Rayleigh Fading Channels," in *Military Commun. Conf.,* 2006, pp. 1-5.

[22] M. Chiani, D. Dardari, and M. K. Simon, "New exponential bounds and approximations for the computation of each error probability in fading channels," in *IEEE Wireless Commun.*, vol. 2, 2003, pp. 840-845.